STRUCTURAL CONTROL AND HEALTH MONITORING
Struct. Control Health Monit. 2008; **15**:299–314
Published online 11 March 2008 in Wiley InterScience
(www.interscience.wiley.com) DOI: 10.1002/stc.250

Movable guyed masts affected by wind loads: Buckling and stochastic response

M. Gioffrè*,†, N. Cavalagli and V. Gusella

Department of Civil and Environmental Engineering, University of Perugia, Via G.Duranti, 93, 06125 Perugia, Italy

SUMMARY

This paper presents a new structural system to be used in communication towers and demonstrates the achieved improved structural performances with respect to currently used cable-stayed masts. The proposed structure is a cable-stayed tower where a truss system is introduced as a new link between the cables and the mast in order to improve the lateral stiffness and to reduce instability phenomena. The motivations and the main design choices for such a supporting structure are outlined. Numerical models are developed in order to accurately describe the geometrically nonlinear behavior of both the cables and the whole system. A combined linear/nonlinear stability analysis is proposed to investigate the structural stability of the system and the Monte Carlo simulation approach is used to estimate the stochastic response of the supporting structure to a correlated Gaussian vector describing the wind load. The obtained results manifest the better performances achievable by introducing the truss system. Copyright © 2008 John Wiley & Sons, Ltd.

KEY WORDS: cable-stayed mast; geometrically nonlinear behavior; buckling; stochastic response; correlated Gaussian load; Monte Carlo simulation

1. INTRODUCTION

Mobile phones are connected to the mobile and fixed phone networks using systems named 'base stations'. These are mainly composed of the supporting structure, the communication devices (antennas and/or dishes), and the shelter used to place the equipment for controlling and running the transmission apparatus. Some of these base stations are designed to be easily removed and placed somewhere else to accommodate the required volume of users at any given area at different times of the year.

*Correspondence to: M. Gioffrè, Department of Civil and Environmental Engineering, University of Perugia, Via G.Duranti, 93, 06125 Perugia, Italy.
†E-mail: mami@unipg.it

Contract/grant sponsor: Italian Ministry for Scientific Research (MIUR)-Cofin 2004 Research Project

Received 15 February 2007
Revised 18 December 2007
Accepted 27 December 2007

The main features of the supporting structure of such stations are the lightweight and the slenderness that make wind the prevalent load and shift the leading concerns in the design process onto the assessment of the structural stability and the mechanical damage due to stress fluctuations (fatigue). Furthermore, the estimation of the peak response becomes crucial if one considers the severe requirements in terms of maximum displacements and rotations of the antennas which have to be satisfied for the radio signals to be successfully transmitted.

Within this context, a research project was started to address the problems arising when designing, constructing, and maintaining such structures. In the first stage of the research, two structural layouts were investigated by experimental tests. One will be referred to as the original structure (OS) and is a typical cable-stayed mast with six orders of stays placed at 120° angle from each other [1]; the other will be indicated as the new structure (NS) and is obtained by modifying the connections between the cables and the post [2]. In particular, a truss system is used which changes the internal forces distribution overcoming serious problems in terms of structural stability and improving the overall dynamic behavior.

The main goal of this paper is to investigate the effect of the truss system on two main aspects: first the structural stability and second the stochastic response of the two systems when affected by a correlated Gaussian vector process describing the wind action. Suitable numerical finite element models (FEM) are developed accounting for the geometrically nonlinear behavior of the cables, and the Monte Carlo simulation is performed on the two systems in order to compare the main response statistics.

2. STRUCTURAL SYSTEMS

One of the problems associated with movable base stations is the need to reduce, as much as it is possible, the plan dimensions both for facilitating the transport and for simplifying all the bureaucratic procedures to obtain installation permissions (e.g. Italy). This design requirement leads to disadvantageous structural features associated with the stays being at a large angle with the ground, thus reducing their effectiveness in terms of overall stiffness and stability.

The problem described so far motivated a significant change in the original structural design. The stays, which are usually directly connected to the mast (Figure 1), are now linked to a special truss system as it is shown in Figure 2. The obtained structural layout very closely resembles a sailing boat mast. It is expected that this configuration increases the stiffness and induces a more uniform distribution of internal forces, thus improving the overall performance in terms of both displacements and stability.

The two structural systems analyzed in this paper are shown in Figures 1 and 2. They have exactly the same geometric and material properties but the truss system. The mast is made of five steel elements, length of 6 m and pipe cross section, connected by bolted flanges. The lower four elements have a diameter of 168.3 mm and a thickness of 12.5 mm. The higher element has a diameter of 139.7 mm and a thickness of 10.0 mm. There are five orders of three stays, the directions of which form 120° angles in the plan view. The lower part of the mast is connected to a shelter in two locations (heights 0.93 and 3.76 m) and two pipe steel rods (thickness 10 mm) connect the upper part of the shelter frame to the post, increasing its lateral stiffness. The foundation slab is made of three precast elements, mixing steel beams and reinforced concrete, with plan dimension of 7.2 m × 5.0 m and thickness of 30 cm.

DOI: 10.1002/stc

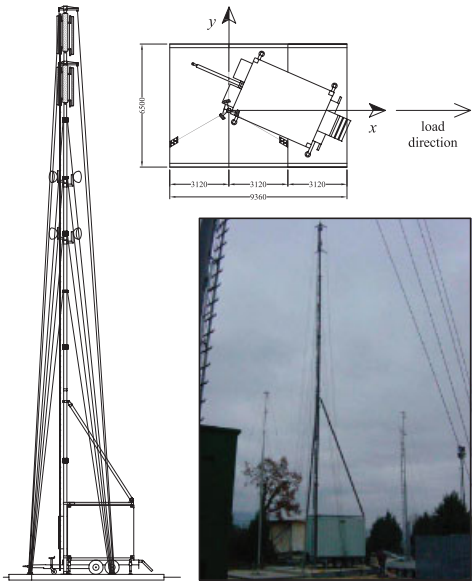

Figure 1. Original structure (no truss system).

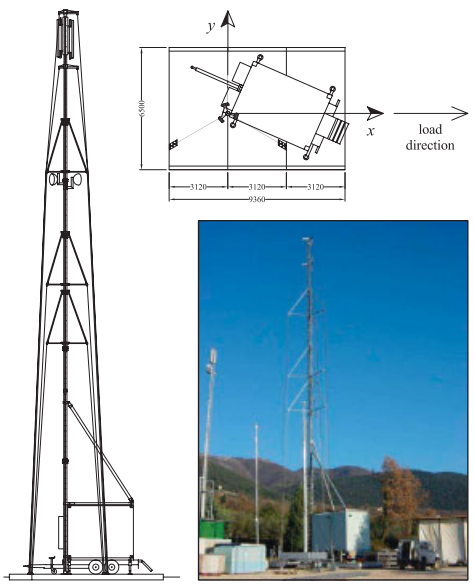

Figure 2. New structure (truss system).

The only difference in the new supporting structure is the introduction of the two-elements truss system with rectangular steel tube section (dimensions 60 mm × 40 mm, thickness 3 mm) in the first three orders of stays. One of the elements is horizontal and mainly carries compression force, whereas the other is diagonal and principally bears tensile force. Further

DOI: 10.1002/stc

information on the actual structural system is beyond the scope of this paper and can be found in [2] together with the results of experimental tests aimed at characterizing and identifying its mechanic and dynamic behaviors.

3. NUMERICAL MODELING

The structural response is calculated developing a suitable numerical code based on the FEM, which takes into account the inherent geometrically nonlinear behavior of the cables and the whole systems [3].

The solution of such nonlinear problems can be obtained by the incremental approach where the loads are applied by increments and the corresponding deformations are calculated. The equilibrium equation of a body at time $t+\Delta t$ can be obtained using the principle of virtual displacements referring to a known configuration t_r:

$$\int_{{}^{t_r}\Omega} {}_{t_r}^{t+\Delta t}S_{ij}\,\delta\,{}_{t_r}^{t+\Delta t}\varepsilon_{ij}\,\mathrm{d}^{t_r}\Omega = {}^{t+\Delta t}\mathscr{R} \tag{1}$$

where S_{ij} is the second Piola–Kirchhoff stress tensor, ε_{ij} is the Green–Lagrange strain tensor [4], and ${}^{t+\Delta t}\mathscr{R}$ is the external load. The integral is performed over a known domain ${}^{t_r}\Omega$. The undeformed or any of the known intermediate equilibrium configurations can be used as reference. In this paper, the updated Lagrangian approach is adopted in which the last calculated equilibrium configuration (at time t) is chosen as reference [5]. Equation (1) is, in general, nonlinear because of possible nonlinearities in the constitutive and/or compatibility equations and can be expressed defining the involved kinematic and static variables as the sum of a known value and an unknown increment. This increment can be linearized about the last calculated configuration and finally, using appropriate shape functions to interpolate the displacement field, the equilibrium equation can be expressed as

$$({}_t^t\mathbf{K}_{\mathrm{L}} + {}_t^t\mathbf{K}_{\mathrm{NL}})\Delta_t^{t+\Delta t}\mathbf{u} = {}^{t+\Delta t}\mathbf{R} - {}_t^t\mathbf{F} \tag{2}$$

where the matrices ${}_t^t\mathbf{K}_{\mathrm{L}}$ and ${}_t^t\mathbf{K}_{\mathrm{NL}}$ are the elastic and geometric components of the tangent stiffness matrix ${}_t^t\mathbf{K}_{\mathrm{T}}$. The vector $\Delta_t^{t+\Delta t}\mathbf{u}$ is an approximation of the nodal displacement increment from t to $t+\Delta t$. The right-hand side represents the out-of-balance load vector, namely, the load vector that is not yet balanced by the element internal stresses ${}_t^t\mathbf{F}$. In particular, ${}^{t+\Delta t}\mathbf{R}$ represents the applied load vector at time $t+\Delta t$, which can include static, inertia, and damping forces.

Starting from the 2D element already proposed in [6], a straight beam 3D finite element is developed assuming that, during deformation, the cross sections remain plane, the beam can undergo large deflections and rotations, but the deformation is small and the shear deformation is negligible. Under the specified conditions, the stiffness variations are only dependent on orientation variations, and the displacement field is completely characterized by the beam axis deflection, the axial displacements, and the torsional rotation along the axis length. Moreover, linear growths for the axial displacements and torsional rotations are assumed. It follows that the axis deformed configuration is characterized by 12 nodal displacements.

Both static and dynamic analysis are carried out using (2) with the 3D straight beam stiffness matrices and developing a suitable solver engine based on the Newton–Raphson method [7] to tackle the nonlinearity and the Newmark method [5] for the time domain integration. The beam consistent-mass matrix is evaluated from the shape functions with the standard assumption of

DOI: 10.1002/stc

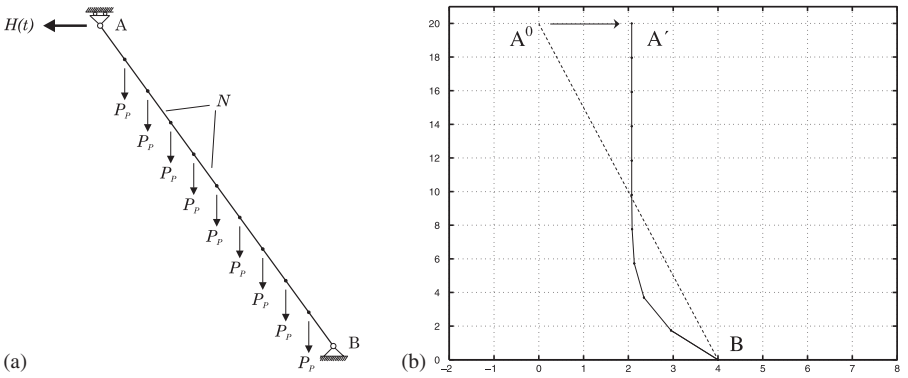

Figure 3. Cable modeling: (a) initial configuration and (b) final configuration.

uniform mass distribution along the beam length and the damping matrix is calculated using the Rayleigh model.

A crucial point is the choice of cable modeling. It seems appealing to use the same beam element described before for the whole structure. In order to accurately describe the highly nonlinear behavior of the stays, it is chosen to use an appropriate number of elements for each cable and give the actual geometrical and mechanical characteristics. In particular, it is found that modeling each of the stays with 10 elements can accurately describe the cable behavior without the need of special finite elements and/or procedures to model the typical compression and bending stiffness that are about zero. As an example, a dynamic analysis is performed on a simply supported cable, loaded with the horizontal force $H(t)$ at the support A (in order to give the initial axial force N, pretension, to the cable) and the self weight P_P, lumped on the nine joints (Figure 3(a)). The cable is released in the horizontal direction at support A, linearly decreasing the pretension to zero. After that, the cable motion under its self weight is followed. The cable starts its motion from the initial configuration shown in Figure 3(a) and finds the equilibrium position reported in Figure 3(b). The obtained response time history together with the configuration at the equilibrium position demonstrates the ability of the numerical model to describe the cable's geometrically nonlinear behavior, in particular, the flying-stay configuration.

In order to compare the effect of the truss system on the structural response, two numerical models are used (Figures 4(a) and (b)). Only the first three orders of stays of the structures shown in Figures 1 and 2 are considered, neglecting the higher two, which are directly connected to the post in both structures. A simplified model for the shelter and the two pipe rods is also used and the effects of the structure–foundation–soil interaction are neglected since they are not crucial in the comparison under investigation. Both models use 15 elements for the mast and 10 elements for each of the cables that are considered pre-tensioned with a force of 5 KN simulating a severe working condition with 50% of cable slackening from the original design pre-tension.

The properties (mechanic and dynamic) of these numerical models were identified using the on-site experimental data obtained in [2].

The main action to be concerned about when dealing with such lightweight and slender structures is the wind load whose instantaneous along-wind velocity is modeled as a correlated,

DOI: 10.1002/stc

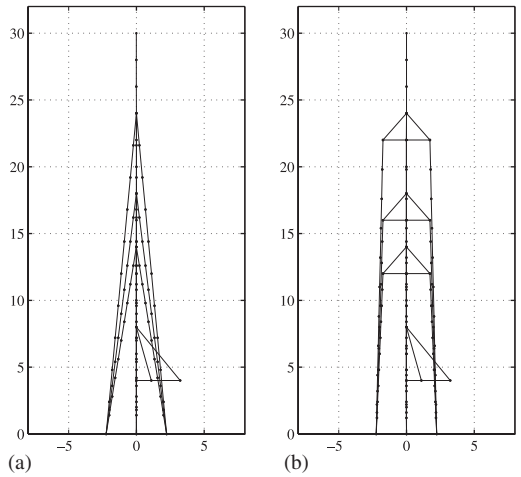

Figure 4. 3D numerical models: (a) OS elevation and (b) NS elevation.

Gaussian, stationary stochastic n-variate vector process with components [8]:

$$V(z_i,t) = \bar{V}(z_i) + v(z_i,t), \quad i = 1,\ldots,n \tag{3}$$

where $\bar{V}(z_i)$ is the mean wind speed at height z_i, and $v(z_i,t)$ is the along-wind turbulence component at height z_i. The cross-power spectral density function between two points on the mast at heights z_i and z_j is given by

$$S_v(z_i,z_j;f) = \sqrt{S_v(z_i;f)S_v(z_j;f)}\mathrm{Coh}(z_i,z_j;f), \quad i,j = 1,\ldots,n \tag{4}$$

where the coherence function is the one proposed by Davenport [9]:

$$\mathrm{Coh}(z_i,z_j;f) = \exp\left[\frac{-2f\sqrt{C_z^2(z_i-z_j)}}{\bar{V}(z_i)+\bar{V}(z_j)}\right], \quad i,j = 1,\ldots,n \tag{5}$$

C_z being the exponential decay coefficient, and the power spectrum of the longitudinal turbulence at height z_i is [10]

$$S_v(z_i;f) = \frac{\sigma_v^2(z_i)}{f}\frac{6.868\tilde{f}(z_i)L_v(z_i)/z_i}{(1+10.302\tilde{f}(z_i)L_v(z_i)/z_i)^{5/3}}, \quad i = 1,\ldots,n \tag{6}$$

where $\tilde{f}(z_i) = fz_i/\bar{V}(z_i)$ is the reduced frequency, $L_v(z_i)$ is the integral length scale of turbulence, and $\sigma_v(z_i)$ is the turbulence standard deviation.

The boundary layer is modeled as far as open country exposure, using the parameters suggested by CEN [11].

Samples of the velocity time histories are generated using a procedure based on the sampling theorem [12] proposed in [13]. In particular, correlated wind speed fluctuations at $n = 15$ locations (model joints of the mast) along the structure's height are simultaneously generated to load the structural model using

$$F(z_i,t) = 0.5\rho AC_pV(z_i,t)^2, \quad i = 1,\ldots,n \tag{7}$$

DOI: 10.1002/stc

where A is the tributary area, ρ is the air mass density, the pressure coefficients, C_p, are considered constant neglecting the effect of the flow–structure–truss system interactions, and the wind load on the cables is not considered because of its limited amplitude.

4. STABILITY ANALYSIS

Given the lightweight and the slenderness of the structures under investigation, large displacements and nonlinear load–displacement curves exhibiting softening or the snap-through phenomenon (i.e. system suddenly going into a different equilibrium state far away from the initial configuration, see Von Mises truss in [14]) are expected. A stability analysis of these types of structures aims at the estimation of the load level that causes considerable deformation or that initiates the snap-through, the nonlinear critical load $P_{\mathrm{cr}}^{\mathrm{NL}}$, that can be obtained accurately only with time-consuming geometrically nonlinear analysis.

As an alternative approach, let the configuration at time t be the fundamental equilibrium state where ${}^{t}\mathbf{R} = {}_{t}^{t}\mathbf{F}$. The instability limit is reached when there exists an adjacent equilibrium configuration at time $t + \Delta t$ with the same load level ${}^{t+\Delta t}\mathbf{R} = {}_{t}^{t}\mathbf{F}$ that makes Equation (2) homogeneous and leads to the condition

$$\det[{}_{t}^{t}\mathbf{K}_{\mathrm{T}}] = 0 \tag{8}$$

for the fundamental equilibrium state at the arbitrary time t, indicating that the tangent stiffness matrix is singular at the critical load level (i.e. the nodal displacements vector increases toward infinity for an infinitesimal increment of the load vector). The solutions of (8) can be found with several linear eigenvalue analyses differing in the assumption on the relationship between the load parameter ${}^{t}\lambda$ and the elements of ${}_{t}^{t}\mathbf{K}_{\mathrm{T}}$. The most used formulations of this problem are

$$\det[{}^{0}\mathbf{K}_{e} + {}_{t}^{t}\mathbf{K}_{u} + {}^{t}\lambda\, {}_{t}^{t}\mathbf{K}_{\mathrm{NL}}] = 0 \tag{9}$$

and

$$\det[{}^{0}\mathbf{K}_{e} + {}^{t}\lambda({}_{t}^{t}\mathbf{K}_{u} + {}_{t}^{t}\mathbf{K}_{\mathrm{NL}})] = 0 \tag{10}$$

where the elastic component ${}_{t}^{t}\mathbf{K}_{\mathrm{L}}$ of the tangent stiffness matrix has been divided into the two contributions of the linear elastic stiffness matrix in the initial configuration (non-deformed) ${}^{0}\mathbf{K}_{e}$ and the stiffness matrix depending linearly on the nodal displacement vector ${}_{t}^{t}\mathbf{K}_{u}$. Both formulations give the classical linear buckling analysis if the fundamental equilibrium position is the undeformed configuration where the initial displacement matrix ${}_{t}^{t}\mathbf{K}_{u}$ vanishes.

Equations (9) and (10) give accurate critical load predictions only if the structural system has a linear prebuckling path but can also be applied to structures with a nonlinear behavior with a bifurcation or a limit value giving estimates that can be both conservative and overestimated. Brendel and Ramm [15] proposed to combine the nonlinear and linear buckling analysis, estimating the critical value for different fundamental equilibrium configurations (at load levels ${}^{t}\mathbf{R}$) obtaining a curve of estimates that would intersect the nonlinear load–deflection diagram at the value initiating the instability, if it exists. The shape of this curve also indicates the degree of nonlinearity of the prebuckling behavior. Chang and Chen [16] applied this combined analysis on a group of 12 structures obtaining curves varying considerably in shape when using (9) while having significantly less variations when using (10). In the latter case, it was possible to obtain predictions of the stability limit of the structure, accurate for practical design purposes, using

DOI: 10.1002/stc

a linear extrapolation based on two values of the estimated critical load, thus reducing the number of nonlinear analyses.

One of the reasons motivating the introduction of the truss system for the structures investigated in this work can be introduced by comparing its different response to wind action. Figure 5 shows the displacements and bending moment diagrams, at a generic time t, of the two systems affected by a sample of the correlated wind forces described in the previous section. The bending moment distribution changes dramatically because of the combined effect of the diagonal and horizontal elements of the truss system that carry mainly tensile and compression forces, respectively. In particular, this effect determines the inversions from positive values to negative values, which are not present in the bending moment diagram of the OS. It follows that higher values of the instability level are expected given the reduction of the effective length associated with the bending moment inversions. This expectation can be demonstrated with a simple test case. The structural model is a simply supported beam under axial load P with the classical critical linear buckling load given by the Euler load P_{E}. Two different perturbations are given on this structure to obtain bending moment distributions that are similar in shape to those of Figures 5(b) and (d): the first is a series of joint loads F, orthogonal to the beam axis, case 1 (Figure 6(a)), and the second adds to case 1 three pairs of joint loads F_c, case 2 (Figure 6(b)). In order to estimate the nonlinear buckling load, a new algorithm is proposed. First, the perturbation is applied and the corresponding equilibrium position is assumed as the fundamental state at time t_v evaluating the tangent stiffness matrix ${}^{t_v}_{t_v}\mathbf{K}_{\mathrm{T}}$. Second, different axial load levels, $\mathbf{P} = {}^{t}\mathbf{R}$, are applied and the corresponding tangent stiffness matrix ${}^{t}_{t}\mathbf{K}_{\mathrm{T}}$ is calculated at equilibrium. Finally, the linear critical load predictions for each of the axial load levels are performed using

$$\det[{}^{t_v}_{t_v}\mathbf{K}_{\mathrm{T}} + {}^{t}\lambda({}^{t}_{t}\mathbf{K}_{\mathrm{T}} - {}^{t_v}_{t_v}\mathbf{K}_{\mathrm{T}})] = 0 \tag{11}$$

which represents a slight modification of Equation (10) and seeks the load level beyond the fundamental state at t_v so that the stiffness ${}^{t_v}_{t_v}\mathbf{K}_{\mathrm{T}}$ is completely degraded by the increments of the elastic and geometric matrices. Figures 6(c) and (d) show the results of the combined linear–nonlinear stability analysis using (9) and (11) plotting the predicted critical loads $P_{\mathrm{cr}}^{\mathrm{NL}}$ against the applied axial load P so that the shape of these curves does not depend on the selected degree

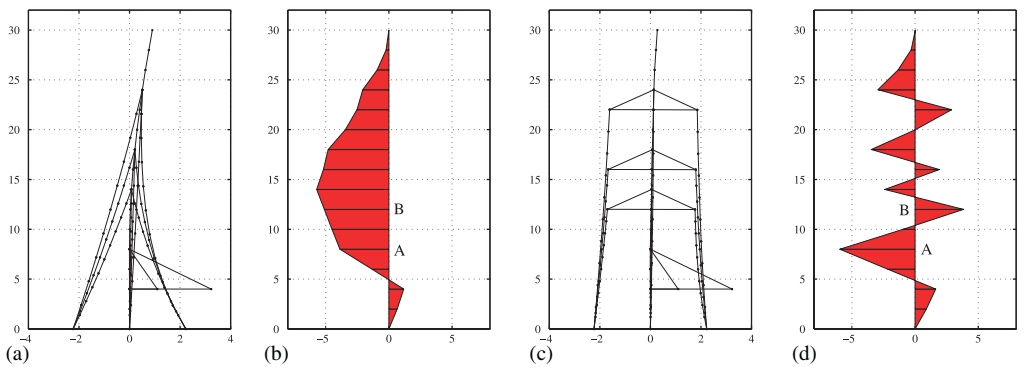

Figure 5. Snapshot of the animation describing displacements and bending moment time series: (a) OS displacements; (b) OS bending moment; (c) NS displacements; and (d) NS bending moment.

DOI: 10.1002/stc

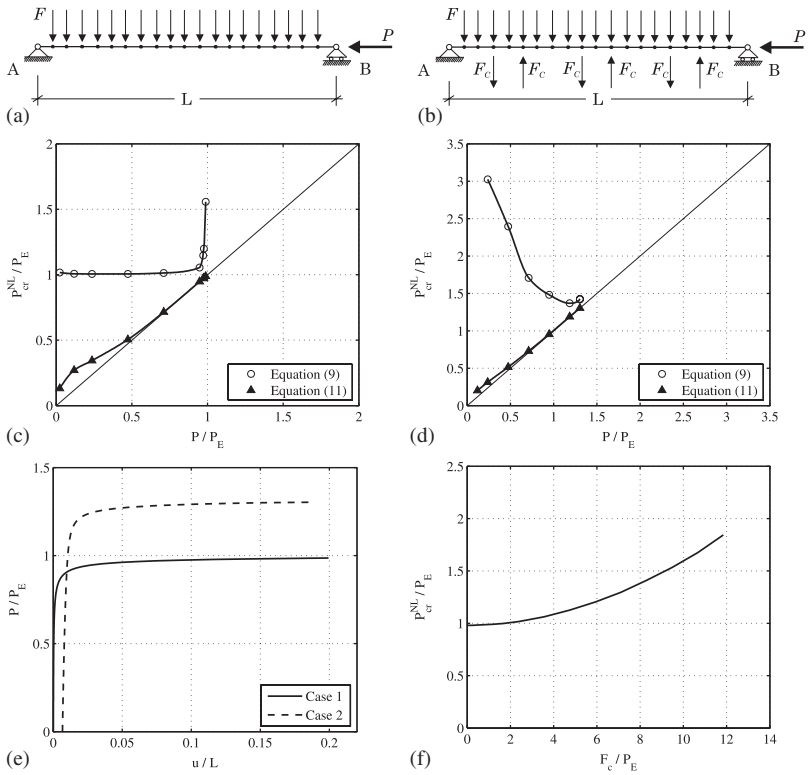

Figure 6. Test cases: (a) model for case 1; (b) model for case 2; (c) estimated P_{cr}^{NL}, case 1; (d) estimated P_{cr}^{NL}, case 2; (e) load–deflection diagrams; and (f) effect of the forces F_c on the estimated P_{cr}^{NL}.

of freedom and the instability occurs at the point of coordinates (P_{cr}^{NL}, P_{cr}^{NL}). These results are consistent with the findings in [16] since the curves obtained with (9) turn sharply near the expected critical load and those evaluated with (11) are very close and parallel to the 45° line, both indicating that no instability occurs. In these cases, it is always possible to extrapolate the obtained curves to predict the critical load to be used for practical design purposes since the deflections become unacceptably large as it is shown in Figure 6(e) for the horizontal displacement u at the support in B. It is worth noting that the predicted critical load for case 2 is an increasing function of the magnitude of F_c as it is shown in Figure 6(f). The results reported in Figures 6(c)–(e) are obtained for $F_c/P_E = 7.1$.

The procedure used to analyze the previous cases is now used on the numerical models of Figure 4. In this case the axial load is applied at the free end of both structures ($-z$ direction in Figures 1 and 2) and the perturbation is given by the wind action (x direction) considered as the equivalent static loads on the mast joints given by [11] for open country exposure. Figure 7(a) shows the predicted critical load curves obtained using (9) and (11) on the two structural models. The significant beneficial effect of the truss system on the estimated P_{cr}^{NL} (about 20 and 52 kN for OS and NS, respectively) and the nonlinear behavior of the two systems before this load level are rather evident. In this case, the complexity of the investigated structures influences the shapes of the predicted curves that deviate from the straight line also when using (11).

DOI: 10.1002/stc

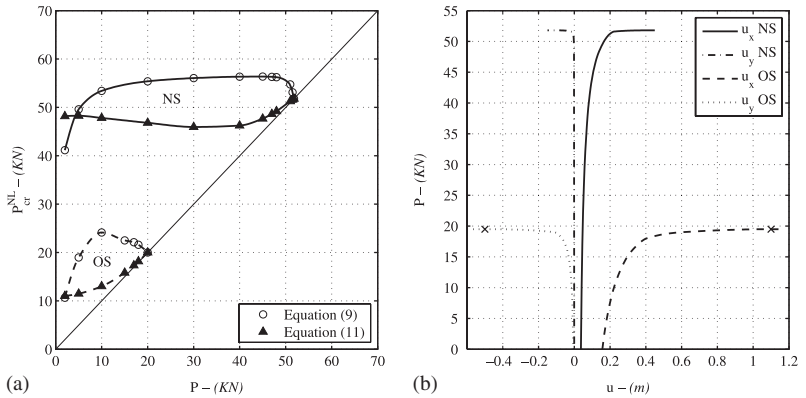

Figure 7. Linear–nonlinear analysis: (a) estimated P_{cr}^{NL} and (b) load–deflection diagrams.

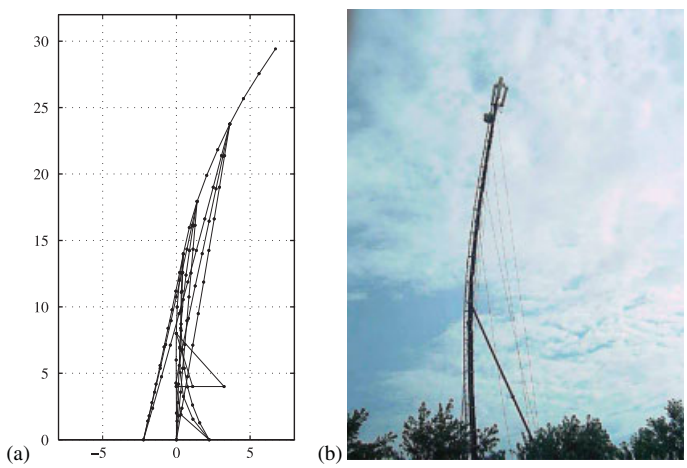

Figure 8. Case of instability for OS: (a) numerical model and (b) actual configuration.

The linear extrapolation proposed in [16] should, therefore, be modified with extrapolation of higher orders that can still be based on a limited number of nonlinear analysis. The axial-load–deflection diagrams, which are shown in Figure 7(b) for the displacements of the free end in the x and y directions of Figures 1 and 2 testify both the nonlinear behavior of the structures and the increase of the stiffness given by the truss system. Furthermore, both the numerical models reach an axial load level where the nodal displacements increase considerably. In this study, it is not possible to verify whether or not a snap-through phenomenon is occurring since the developed solver is based on the Newton–Raphson algorithm, but it can clearly be stated that a critical load level is obtained, which initiates large deformations. Figure 8 bears out this last statement. Figure 8(a) reports the calculated configuration for the OS at a time where the load–deflection curve exhibits a plateau region where the structure is very flexible with some flying stays (point marked with (x) in Figure 7(b)), while Figure 8(b) shows a configuration of the actual structure during its service life. Both figures testify the existence of an equilibrium position far off the designed undeformed configuration. It is worth noting that to completely

DOI: 10.1002/stc

investigate the actual stability of the structural systems analyzed in this paper, the dynamic equilibrium should be considered given the non-conservative nature of the wind action, which may induce unbounded motion rather than having the system going into another equilibrium state.

5. STOCHASTIC ANALYSIS

The main stochastic features of the structural response are estimated using the Monte Carlo approach under the assumption of ergodic process. The stationary response is, therefore, evaluated for a single time series of the wind vector process (7) applied in the x direction of both models (Figures 1 and 2) and performing the numerical integration of the dynamic equilibrium equations for a duration of 10 min with a time step of 0.02 s (30 000 samples). This procedure permitted to save a notable amount of time that would have been otherwise required in order to perform ensemble averages, given the complexity of the analysis and the need to discharge the initial transient response.

The first 60 s of the stationary response displacements time histories at the free end of the two structures in both x and y directions are shown in Figures 9(a) and (b), whereas the corresponding power spectral densities of the normalized series (zero mean and unit variance) are reported in Figures 9(c) and (d). The different behavior caused by the truss system is confirmed both in the response amplitudes and the resonant peaks. The dynamic response is dramatically reduced by the truss system for the combined effect given by the increased stiffness on the static displacements and the system's natural frequencies. Figures 9(e) and (f) effectively demonstrate the different behavior in the x–y plane showing the trajectories of the free end of both structures in the same scale. Figures 9(a), (b) and 9(e), (f) also show a special effect of the truss system on the cross-wind fluctuations that are in the same order of magnitude as the along-wind oscillations in the OS, while they are almost cancelled out in the NS.

In order to have information on the stochastic features associated with the effect of the truss system on the bending moment distribution, the cross-covariance functions of two bending moment time series in sections (A) and (B) in Figure 5 were estimated. Figure 10 clearly shows the differences in the two structural models. In particular, the two sections considered experience the same bending moment sign (positive covariance at $\tau = 0$) in the OS (Figure 10(a)) and opposite sign (negative covariance at $\tau = 0$) when the truss system is introduced (Figure 10(b)). Furthermore, the values of the joint bending moments are less dispersed in the NS. This can be highlighted more completely if the joint probability density functions (JPDFs) are estimated (Figure 11).

Other interesting information on the stochastic response of the two structures comes from the analysis of the displacements. Table I reports the first four statistical moments (mean μ, standard deviation σ, skewness γ_3, and kurtosis γ_4 coefficients) of the displacements at the free end of the structures. These results confirm the reduction of the response amplitudes and also manifest a significant reduction of the response variability, especially in the cross-wind displacements. The skewness and kurtosis coefficients indicate a slight deviation from the Gaussian model, which should be associated with the nonlinear structural behavior. Within this context, the truss system seems to keep the NS closer to the linear behavior for the considered wind action. The results obtained for the cross-wind response of the NS differ significantly from the others. At a first look these results might suggest a strong deviation from the Gaussian model, but the variance of this fluctuations has such a small amplitude that this process might be considered almost deterministic.

DOI: 10.1002/stc

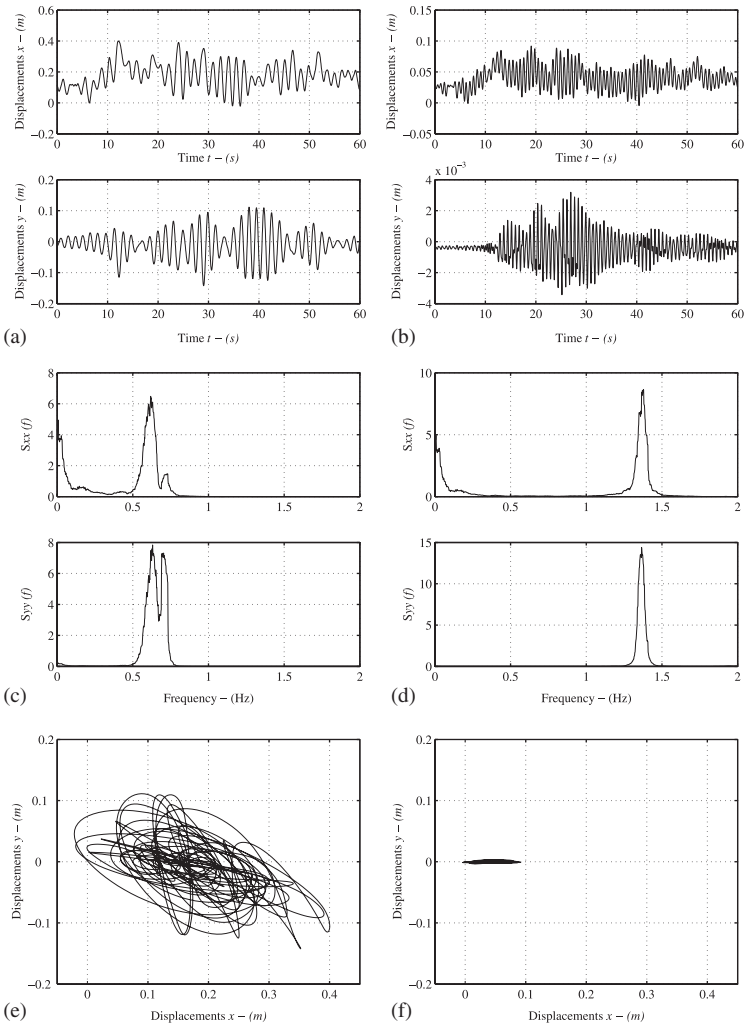

Figure 9. Dynamic response: time histories of the x (above) and y (below) displacements at the free end of (a) OS, (b) NS; power spectral densities of the x (above) and y (below) displacements at the free end of (c) OS, (d) NS; trajectories of the free end in the two models: (e) OS, (f) NS.

Figure 12 shows estimates of the marginal probability density functions (MPDFs) of the processes described so far (histograms) together with the Gaussian density function (continuous line) estimated from the first two statistical moments. All these response probabilistic features have to be carefully considered when peak values and fatigue analysis are of interest.

Additional information useful to compare the stochastic response differences is provided by Figure 13 with the estimates of the joint probability density functions between the displacements x and y at the free end of the structures. This figure confirms that the truss system makes the response more likely to be confined in the along-wind plane with respect to the original system.

DOI: 10.1002/stc

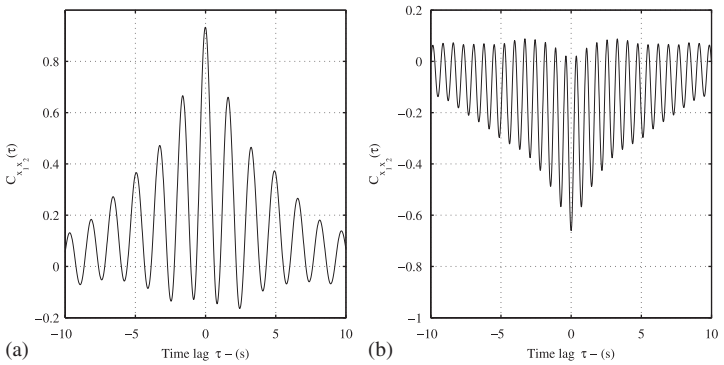

Figure 10. Cross-covariance functions for the moment time series in A and B (Figure 5): (a) OS and (b) NS.

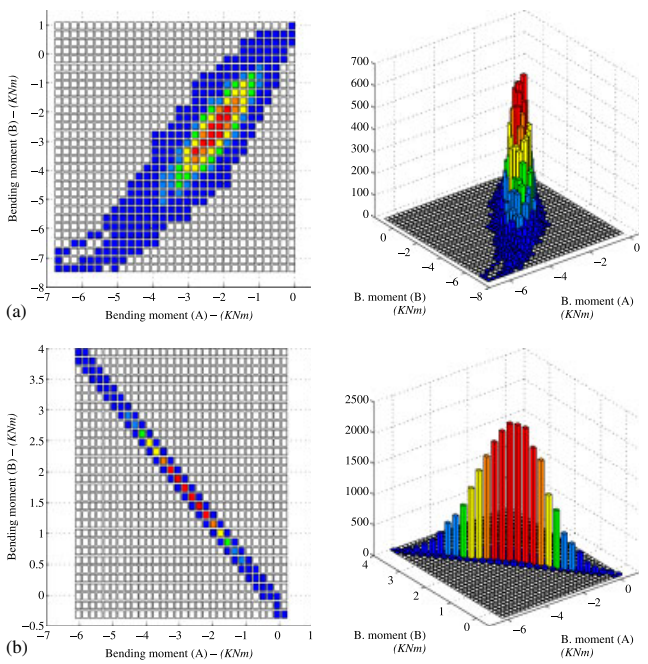

Figure 11. JPDFs for the bending moment time series in A and B (Figure 5): (a) OS and (b) NS.

6. CONCLUSIONS

A new structural system to be used for cable-stayed communication towers is presented in this paper and its performances are compared with currently used cable-stayed masts in terms of stability and stochastic features. A preliminary description of the OS and the motivations of the structural changes introducing a truss system were briefly reported. In order to evaluate the structural response of the two systems, suitable nonlinear numerical models were developed and identified using on-site experimental tests. A combined linear–nonlinear approach that should

DOI: 10.1002/stc

Table I. Statistical moments of the displacements at the free end of the structures.

	Original structure		New structure	
	x	y	x	y
μ	0.1686	−0.0095	0.0380	−4.07e − 004
σ	0.0780	0.0482	0.0161	5.91e − 004
γ_3	0.1883	−0.0547	0.1323	0.3504
γ_4	3.1090	2.7716	3.0402	7.5125

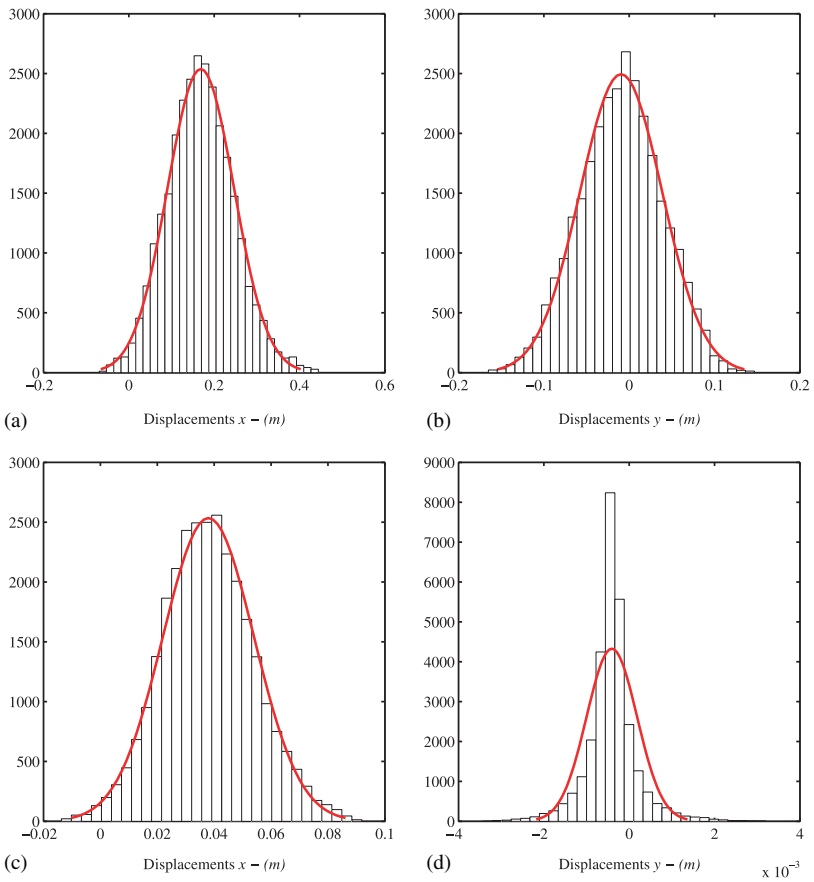

Figure 12. MPDFs of the displacements at the free end: (a) OS x; (b) OS y; (c) NS x; and (d) NS y.

reduce the computation time with respect to fully nonlinear analysis was proposed to estimate the critical loads initiating the static instability. The Monte Carlo approach was used to obtain estimates of the probabilistic features of the structural response. The results' comparison confirmed what was expected in the design stage, i.e. the new cable-stayed mast with the truss system has overall improved behavior when compared with the original one. The results of this

DOI: 10.1002/stc

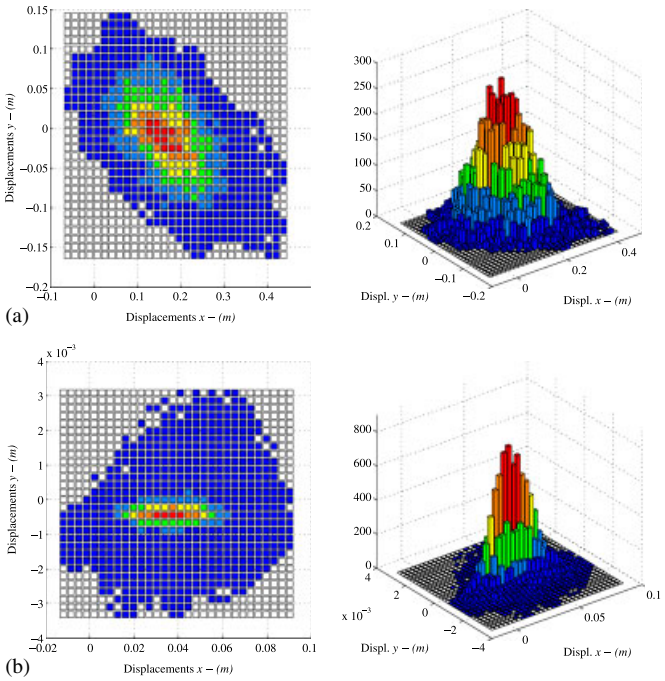

Figure 13. Estimates of the JPDF between x and y displacement fluctuation: (a) OS and (b) NS.

study can be used as a first step in order to estimate the reliability and the managing costs of the two structures, which are other essential parameters for the phone company in order to make a definitive selection of one of the two structural systems. Furthermore, a more complete investigation into the actual stability of the two structural layouts can be obtained by dynamic equilibrium which accounts for the non-conservative nature of the wind action. Finally, the obtained results can also be used to design control strategies in order to further reduce the dynamic displacements and rotations and satisfy the severe serviceability limit states imposed by the phone companies.

ACKNOWLEDGEMENTS

This work was supported by the Italian Ministry for Scientific Research (MIUR)-Cofin 2004 Research Project and CAEL s.r.l (Rome, Italy). The authors are grateful to Ing. Stefano Morbidoni of Elettromontaggi s.r.l. for his useful comments and criticism and for providing the picture in Figure 8(b).

REFERENCES

1. Gioffrè M, Gusella V, Materazzi AL, Venanzi I. Removable guyed mast for mobile phone networks: wind load modeling and structural response. *Journal of Wind Engineering and Industrial Aerodynamics* 2004; **92**(6):463–475.
2. Gioffrè M, Gusella V, Morbidoni S. Identification of a special class of removable guyed mast. *Proceedings*, *Sixth European Conference on Structural Dynamics* (*EURODYN 2005*), Paris, France, 2005; 2237–2242.
3. Gioffrè M, Gusella V. Numerical analysis of structural systems subjected to non-Gaussian random fields. *Meccanica* 2002; **37**(1–2):115–128.

DOI: 10.1002/stc

4. Malvern LE. *Introduction to the Mechanics of a Continuous Medium*. Prentice-Hall: Englewood Cliffs, NJ, 1969.
5. Bathe K-J. *Finite Element Procedures in Engineering Analysis*. Prentice-Hall: Englewood Cliffs, NJ, 1982.
6. Antonini A, Gioffrè M, Gusella V. Geometrically nonlinear cantilever under stochastic loading vectors. *Nonlinear Dynamics* 2002; **28**(1):83–102.
7. Bonet J, Wood R. *Nonlinear Continuum Mechanics for Finite Element Analysis*. Cambridge University Press: New York, 2000.
8. Simiu E, Scanlan RH. *Wind Effects on Structures*: *Fundamentals and Applications to Design* (3rd edn). Wiley Interscience: New York, 1996.
9. Davenport AG. The dependence of wind loads upon meteorological parameters. *Proceedings of the International Research Seminar Wind Effects on Buildings and Structures*, Ottawa, Canada, 1967; 19–82.
10. Solari G. Gust Buffeting. I: Peak Wind Velocity and Equivalent Pressure. *Journal of Structural Engineering* (ASCE) 1993; **119**(2):365–382.
11. CEN. Eurocode 1: actions on structures—general actions—part 1–4: wind actions. *prEN 1991-1-4:2004*, CEN.
12. Grigoriu M, Balopoulou S. A simulation method for stationary Gaussian random functions based on the sampling theorem. *Probabilistic Engineering Mechanics* 1993; **8**(3–4):239–254.
13. Gioffrè M. Analysis and simulation of non-Gaussian processes with application to wind engineering and reliability. *Ph.D. Thesis*, University of Florence, Florence, Italy, 1998.
14. Bažant ZP, Cedolin L. *Stability of Structures. Elastic*, *Inelastic*, *Fracture and Damage Theories*. Dover: New York, 2003.
15. Brendel B, Ramm E. Linear and nonlinear stability analysis of cylindrical shells. *Computers and Structures* 1980; **12**:549–558.
16. Chang S-C, Chen J-J. Effectiveness of linear bifurcation analysis for predicting the nonlinear stability limits of structures. *International Journal for Numerical Methods in Engineering* 1986; **23**:831–846.

DOI: 10.1002/stc